The Astrophysical Journal, 876:63 (9pp), 2019 May 1 https://doi.org/10.3847/1538-4357/ab15db

First Abundance Measurement of Organic Molecules in the Atmosphere of HH 212 Protostellar Disk

Chin-Fei Lee[1,2], Claudio Codella[3,4], Zhi-Yun Li[5], and Sheng-Yuan Liu[1]
[1] Academia Sinica Institute of Astronomy and Astrophysics, P.O. Box 23-141, Taipei 106, Taiwan; cflee@asiaa.sinica.edu.tw
[2] Graduate Institute of Astronomy and Astrophysics, National Taiwan University, No. 1, Section 4, Roosevelt Road, Taipei 10617, Taiwan
[3] INAF, Osservatorio Astrofisico di Arcetri, Largo E. Fermi 5, I-50125 Firenze, Italy
[4] Univ. Grenoble Alpes, CNRS, Institut de Planétologie et d'Astrophysique de Grenoble (IPAG), F-38000 Grenoble, France
[5] Astronomy Department, University of Virginia, Charlottesville, VA 22904, USA
Received 2019 January 31; revised 2019 April 2; accepted 2019 April 2; published 2019 May 6

Abstract

HH 212 is one of the well-studied protostellar systems, showing the first vertically resolved disk with a warm atmosphere around the central protostar. Here we report a detection of nine organic molecules (including newly detected ketene, formic acid, deuterated acetonitrile, methyl formate, and ethanol) in the disk atmosphere, confirming that the disk atmosphere is, for HH 212, the chemically rich component, identified before at a lower resolution as a "hot corino." More importantly, we report the first systematic survey and abundance measurement of organic molecules in the disk atmosphere within ∼40 au of the central protostar. The relative abundances of these molecules are similar to those in the hot corinos around other protostars and in Comet Lovejoy. These molecules can be either (i) originally formed on icy grains and then desorbed into gas phase or (ii) quickly formed in the gas phase using simpler species ejected from the dust mantles. The abundances and spatial distributions of the molecules provide strong constraints on models of their formation and transport in star formation. These molecules are expected to form even more complex organic molecules needed for life and deeper observations are needed to find them.

Key words: accretion, accretion disks – ISM: individual objects (HH 212) – ISM: jets and outflows – ISM: molecules – stars: formation

1. Introduction

Accretion disks have been detected in very young protostellar systems, feeding the central protostars. With the advent of the Atacama Large Millimeter/submillimeter Array (ALMA), we have started to resolve the disks and study their physical processes in great detail. HH 212 is one of the well-studied protostellar systems, showing the first vertically resolved disk with a warm atmosphere around the central protostar (Lee et al. 2017b, 2017c). This warm atmosphere seems to be the hot corino reported recently at a lower angular resolution (Codella et al. 2016, 2018). Hot corinos are the hot ($\gtrsim$100 K) and compact regions immediately around low-mass (Sun-like) protostars (Ceccarelli et al. 2007), and rich in organic molecules including complex organic molecules (COMs, refering to C-bearing species with six atoms or more; Herbst & van Dishoeck 2009). By determining the connection of the disk atmosphere with the hot corino in HH 212, we aim to determine the origin of the hot corino and the related physical processes in the innermost region. In particular, the nearly edge-on orientation of the disk in this system provides the best view of the atmosphere, allowing us to study the physical properties of the disk atmosphere, and the formation of the organic molecules and their role in producing the rich organic chemistry needed for life.

HH 212 is a young Class 0 protostellar system deeply embedded in a compact molecular cloud core in the L1630 cloud of Orion at a distance of ∼400 pc (Kounkel et al. 2017). The central source is IRAS 05413-0104, with a bolometric luminosity of ∼9 $L_\odot$ (updated for the new distance; Zinnecker et al. 1992). The central protostar has a mass of ∼0.25 $M_\odot$ (Lee et al. 2017c). It drives a powerful bipolar jet (Zinnecker et al. 1998; Lee et al. 2015), which has been recently found to be spinning (Lee et al. 2017a). A rotating disk must have formed around the protostar in order to launch the jet. Our previous ALMA observations toward the center indeed showed a spatially resolved nearly edge-on dusty disk with a radius of ∼60 au (Lee et al. 2017b). In addition, we also detected a warm atmosphere of the disk with a few organic molecules (Lee et al. 2017c), suggesting that the warm disk atmosphere can be the hot corino reported before at a lower resolution (Codella et al. 2016). Recent observations at a resolution of ∼0.″15 (60 au) suggested that deuterated water and CH_3CHO can also reside in the disk atmosphere (Codella et al. 2018). In this paper, we zoom in to the disk region at a higher resolution of ∼0.″03 (12 au) and higher sensitivity and detect additional and more COMs characteristic of a hot corino, with most of them detected for the first time in the disk atmosphere. Our observations confirm that the hot corino in HH 212 is indeed the warm disk atmosphere. We will discuss the formation of the organic molecules by comparing their abundances to those in hot corinos around other low-mass protostars.

2. Observations

The HH 212 protostellar system was observed with ALMA in Band 7 at ∼341.5 GHz in Cycle 5. The project ID was 2017.1.00044.S. Three observations were executed on the same day on 2017 November 27 with 47 antennas, with each observation having an integration time of ∼32.7 minutes on the target. Thus, the total time on the target was ∼98 minutes. The projected baselines were ∼60–8500 m. The correlator was set up to have four spectral windows, with three in continuum mode having a bandwidth of 2 GHz, and one in spectral mode having a bandwidth of 1.875 GHz. In this paper, we only report the results obtained with the spectral mode that covers the rest

frequency from ∼345.635 to 347.510 GHz. The spectral resolution was 1.953 MHz per channel, resulting in a velocity resolution of ∼1.69 km s^{-1} per channel at 346.5 GHz. The primary beam was 17.″27. A single pointing was used to map the system within ∼1″ of the central source. The maximum recoverable size scale was ∼0.″4, enough to map the disk atmosphere without any significant missing flux.

The data were calibrated with the CASA package, with quasar J0510+1800 as a passband and flux calibrator, and quasar J0541-0211 (a flux of 0.137 Jy) as a gain calibrator. We used a robust factor of 0.5 for the visibility weighting to generate the channel maps with a synthesized beam of 0.″036 × 0.″03 at a position angle of ∼−78°. We used the line-free channels to generate a continuum map centered at 356.5 GHz. The channel maps of the molecular lines were generated after continuum subtraction. The noise levels are ∼0.121 mJy beam^{-1} (or ∼1.13 K) in the continuum map and 0.80 mJy beam^{-1} (or ∼7.45 K) in the channel maps. The velocities in the channel maps are LSR velocities.

3. Results

In HH 212, the jet has an axis with a position angle of ∼23° and an inclination angle of ∼4° to the plane of the sky, with its northern component tilted toward us (Claussen et al. 1998). The disk is nearly edge-on and exactly perpendicular to the jet axis (Lee et al. 2017b). The systemic velocity is $V_{\rm sys} = 1.7 \pm 0.1$ km s^{-1} LSR (Lee et al. 2014). In order to facilitate our presentations, we define an offset velocity $V_{\rm off} = V_{\rm LSR} - V_{\rm sys}$ and rotate our maps by 23° clockwise to align the jet axis in the vertical direction.

Figure 1 shows the emission line intensity maps (contours) of nine organic molecules, including CH_3OH (methanol, 4 lines), CH_2DOH (deuterated methanol, 7 lines), $^{13}CH_3OH$ (^{13}C isotopologue of methanol, 1 line, contaminated by a much weaker CH_2DCN line), H_2CCO (ketene, 1 line), CH_3CHO (acetaldehyde, 22 lines), $HCOOCH_3$ (methyl formate, 8 lines), t-HCOOH (formic acid in trans state, 1 line), CH_3CH_2OH (ethanol, 10 lines), and CH_2DCN (deuterated acetonitrile, 5 lines), on the continuum map (color image) of the disk at $\lambda \sim 865$ μm (or equivalently ∼347 GHz), obtained from our observations. As seen before at a similar wavelength ($\lambda \sim 850$ μm) in Lee et al. (2017b), the continuum map shows a "hamburger-shaped" dusty disk with an equatorial dark lane sandwiched between two brighter features on the top and bottom. As discussed in that paper, the presence of the equatorial dark lane is due to relatively low temperature and high optical depth near the disk midplane. As discussed below, the maps of the molecular emissions are obtained by stacking a number of lines (as indicated above in the parenthesis) in different transitions with a range of upper energy levels for better detections. Molecular line emissions are only detected in the upper (above the midplane) and lower disk atmosphere, with the emission brighter in the lower disk atmosphere below the midplane. No molecular emission is detected toward the disk midplane, either because the emission is lost in the optically thick dust continuum emission or because of a lack of emission of these molecules there. All the molecular emissions are detected within the centrifugal barrier (which has a radius of ∼0.″11 or 44 au) of the central protostar. For CH_3OH, CH_2DOH, CH_3CHO, and CH_3CH_2OH, their emissions are clearly detected in the upper and lower atmosphere with a roughly similar distribution, suggesting that they are chemically related. In addition, the emission moves closer to the disk midplane from CH_3OH, CH_2DOH, CH_3CHO, to CH_3CH_2OH, suggesting that the emission of less abundant molecule (see the next section for their abundances) traces deeper into the disk atmosphere, probably due to an optical depth effect. However, it could also be due to a chemical stratification in the vertical direction. CH_2DOH and CH_3CH_2OH emission in the lower atmosphere in the outer edge show a structure curving back toward the midplane, following the lower boundary of the dusty disk emission, likely outlining a physical boundary for the dusty disk.

Figure 2 shows the position–frequency (PF) diagrams obtained with a cut along the lower atmosphere, where the emission is brighter, in order to identify the detections of various molecular lines. The PF diagrams for the upper atmosphere show similar structures but are fainter and thus are not shown here. As can be seen, many lines are detected, with their emission detected within ∼5 MHz of their rest frequencies (or ∼4 km s^{-1} within the systemic velocity) marked by the vertical lines, with one color for each organic molecular species at different transitions. For each line, the diagrams show a roughly linear PF structure with the redshifted emission in the southeast (positive y) and blueshifted emission in the northwest (negative y), as seen before in the corresponding position–velocity diagrams for the CH_3OH and CH_2DOH lines (Lee et al. 2017c). As discussed in that paper, this linear PF structure likely arises from a warm rotating ring of the disk atmosphere near the centrifugal barrier. With this feature, we identify lines from the nine organic molecules mentioned above, and a few other simple molecules (e.g., SO, SO_2, and its isotopologue $SO^{18}O$). Other lines from CO and SiO trace mainly the outflow and jet, and thus do not show such a clear linear PF structure.

Table 1 lists the properties of the organic molecular lines. For each molecular species, we stacked the line intensity maps in different transitions, excluding those tentatively detected (marked with T) and blended (marked with B), producing the mean line intensity map shown in Figure 1.

3.1. Physical Condition in the Disk Atmosphere

Here we derive the mean excitation temperature and column density in the disk atmosphere by fitting the rotation diagram of the molecular lines. This diagram plots the column density per statistical weight in the upper energy state in the optically thin limit, $N_u^{\rm thin}/g_u$, versus the upper energy level E_u of the lines. Here $N_u^{\rm thin} = (8\pi k\nu^2/hc^3A_{ul})W$, where the integrated line intensity $W = \int T_B dv$ with T_B being the brightness temperature.

The emission in the lower disk atmosphere is brighter and is thus used to better derive the mean excitation temperature and column density in the disk atmosphere. Table 1 lists the integrated line intensities in the lower disk atmosphere measured (with a cutoff of 2σ) for the reasonably isolated lines detected with more than 3σ. They are the mean values averaged over a rectangular region that covers most of the emission in the lower atmosphere. Figure 3 shows the resulting diagrams for the six molecules detected with multiple lines. The blended lines are excluded. With the CH_3OH lines, we derived an excitation temperature of ∼160 ± 45 K. With the lines from its deuterated species CH_2DOH, we derived a similar temperature of ∼148 ± 19 K. For a check, we also obtained similar temperatures of ∼138 ± 32 K and ∼168 ± 24 K for the upper atmosphere from the CH_3OH

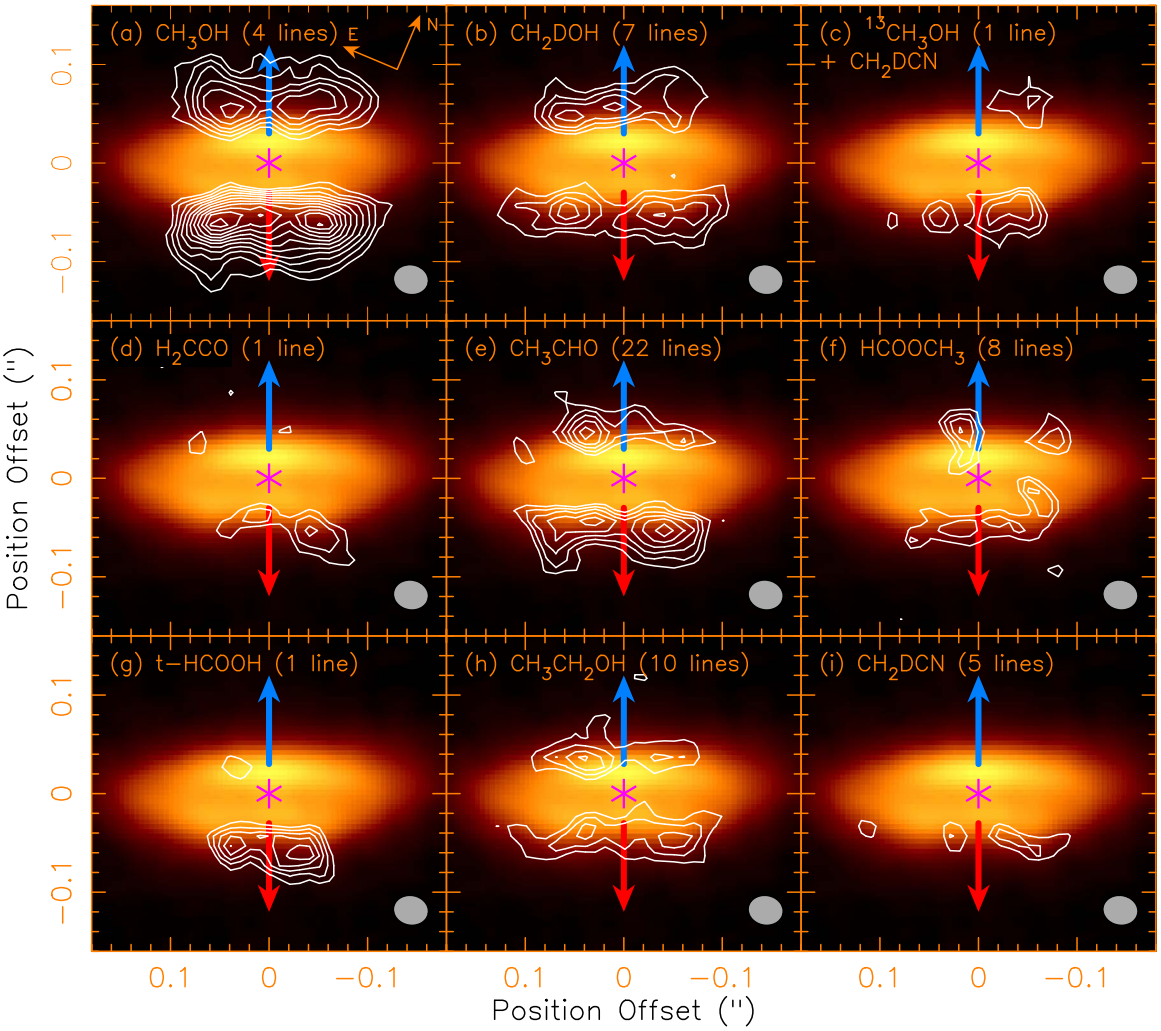

Figure 1. Total emission line intensity maps of nine organic molecules integrated over velocity within ~4 km s^{-1} of the systemic velocity, plotted on top of the continuum map (color image) of the dusty disk. As discussed in the text, the maps of the molecular emissions are obtained by stacking a number of lines (as indicated in the parentheses) in different transitions with a range of upper energy levels for better detections. The asterisk marks the possible position of the central protostar. The blue and red arrows indicate the axes of the blueshifted and redshifted jet components, respectively. The contours start at 3σ with a step of 1σ. The 1σ noise levels in panels (a)–(i) are 1.96, 1.64, 4.06, 3.91, 0.89, 1.10, 4.23, 1.19, and 1.72 mJy beam^{-1} km s^{-1}.

lines and CH_2DOH lines, respectively. The resulting column densities of CH_3OH and CH_2DOH are listed in Table 2. As discussed later, because the CH_3OH lines are likely optically thick, the CH_3OH column derived here is only a lower limit and a more accurate value will be derived using the $^{13}CH_3OH$ column density below.

From CH_3OH and CH_2DOH, we obtain a mean excitation temperature of $\sim 150 \pm 50$ K in the lower disk atmosphere, similar to that found before in Lee et al. (2017c). This mean temperature is also consistent with that derived toward the disk at a lower angular resolution in Bianchi et al. (2017). Assuming this mean temperature for the disk atmosphere, we can estimate the column densities of other molecules with weaker lines. For those molecules detected with multiple lines, such as CH_3CHO, $HCOOCH_3$, CH_3CH_2OH, and CH_2DCN, we can obtain their column densities by fitting their rotation diagrams, as shown in Figures 3(c)–(f). Notice that the column density of CH_3CHO is estimated here to be $(1.5 \pm 0.6) \times 10^{16}$ cm^{-2}, with the lower limit consistent with that estimated previously at a lower resolution with an excitation temperature of $\sim 78 \pm 14$ K in Codella et al. (2018). For those detected with a single line, such as $^{13}CH_3OH$, H_2CCO, and t-HCOOH, we derived their column densities from their measured integrated line intensity. For $^{13}CH_3OH$, the only detected line is contaminated by a weaker line of CH_2DCN and thus its column density is estimated after removing the expected intensity of the CH_2DCN line. The expected intensity of the CH_2DCN line is assumed to be given by the mean intensity of other CH_2DCN lines with similar E_u and $\log A_{ul}$, and it is estimated to be ~21 K km s^{-1}, or ~18% of the total intensity there. Also, as the $^{13}CH_3OH$ line is optically thinner than the CH_3OH lines, we can improve the CH_3OH column density by multiplying the $^{13}CH_3OH$ column density by a $^{12}C/^{13}C$ ratio of 50 as obtained in the Orion Complex (Kahane et al. 2018). As can be seen from Table 2, the CH_3OH column density derived this way is about twice that derived from the rotation diagram, suggesting that the CH_3OH lines are indeed optically thick. Also shown in the table are the column densities of NH_2CHO, D_2CO, and CH_3SH measured in Lee et al. (2017c), adjusted with the mean excitation temperature here.

Based on our disk model that reproduced the dust continuum emission at a similar wavelength of ~850 μm (Lee et al. 2017b), the dust continuum emission in the disk atmosphere has an optical depth $\tau \lesssim 1$. Thus, the derived column densities

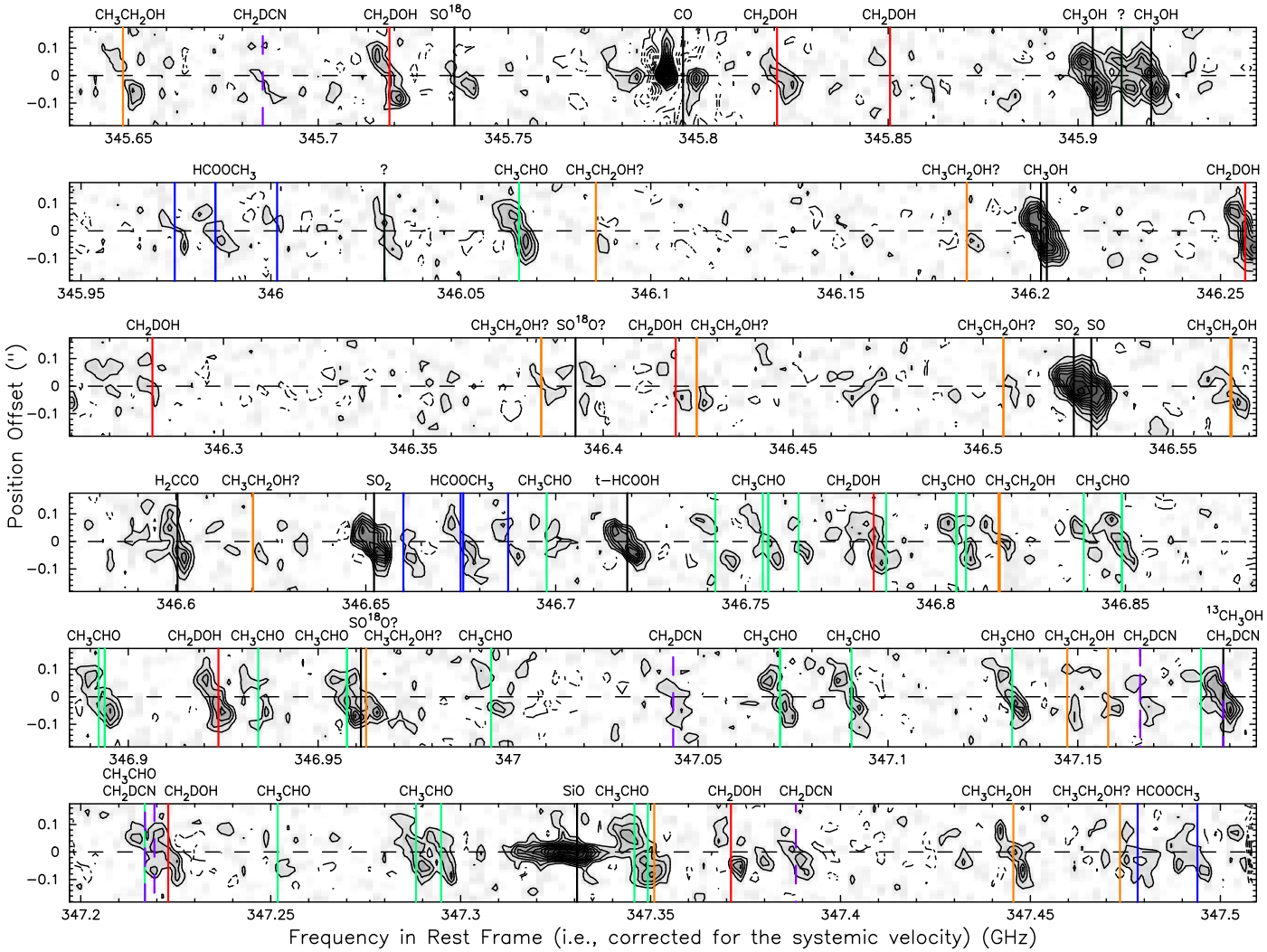

Figure 2. Position–frequency diagrams cut along the lower atmosphere of the disk, in order to show the detections of various molecular lines. The contours start from 2σ with a step of 1σ of 4 K. The frequency has been corrected for the systemic velocity of 1.7 km s^{-1}. The vertical lines mark the rest frequencies of the lines in different transitions, with one color for one organic molecular species. The lines from simple molecules are marked with the black vertical lines. The physical properties of the lines are listed in Table 1.

of the organic molecules could be underestimated by a factor of *e*. In that disk model, the disk atmosphere has a mean H_2 column density of $\sim 3.8 \times 10^{24}$ cm^{-2}. Hence, the abundances of the molecules, as listed in Table 2, can be obtained by dividing the column density of the molecules by this mean H_2 column density. The abundances here can be uncertain by a factor a few because the mean H_2 column density depends on dust opacity, which can be uncertain by a factor of a few.

4. Discussion

4.1. Corino-like Disk Atmosphere

Hot corinos with a temperature $\gtrsim$100 K have been detected around low-mass protostars and they are rich in organic molecules (including COMs). A hot corino has also been recently reported in HH 212 in the inner 100 au with a detection of CH_3CHO and deuterated water HDO (Codella et al. 2016, 2018). Now at higher resolution, we find CH_3CHO to reside in the disk atmosphere. Moreover, we also detect 8 other organic molecules (H_2CCO, t-HCOOH, CH_3OH, CH_2DOH, $^{13}CH_3OH$, CH_2DCN, $HCOOCH_3$, and CH_3CH_2OH) in the disk atmosphere, with an excitation temperature of $\sim 150 \pm 50$ K. Adding 3 other organic molecules (D_2CO, CH_3SH and NH_2CHO) from Lee et al. (2017c), we have 12 organic molecules, with 9 of them being COMs, detected in the disk atmosphere. These results indicate that the hot corino in HH 212 is actually a warm atmosphere of the disk.

4.2. Formation of Organic Molecules

We can study the formation of the organic molecules in the disk atmosphere by comparing their abundances to those estimated in the hot corinos around other Class 0 low-mass protostars. The abundance of CH_3CHO, which is commonly observed in hot corinos, is estimated here to be 3.9×10^{-9} in HH 212, similar to those found in other hot corinos, e.g., 5.8×10^{-9} in IRAS 16293-2422B (Jørgensen et al. 2016), 2.4×10^{-9} in B335 (Imai et al. 2016), and 4.2×10^{-9} in NGC 1333 IRAS4A2 (López-Sepulcre et al. 2017). To facilitate comparison, we calculate and compare the abundances of the organic molecules relative to CH_3CHO. Figure 4 shows the comparison of the relative abundances of seven organic molecules (excluding deuterated species and ^{13}C isotopologue)

Table 1
Line Properties from Splatalogue

Transition QNs	Frequency (MHz)	$\log(A_{ul})$ (s^{-1})	E_u (K)	W[a] (K km s^{-1})	Line List
t−HCOOH 15(2,13)−14(2,12)	346718.85	−3.331	144.457	147	CDMS
H_2CCO 17(1,16)−16(1,15)	346600.45	−3.325	162.789	79	JPL
CH_3OH 16(1)− −15(2)−	345903.91	−4.044	332.653	234	JPL
CH_3OH 18(−3) − 17(−4), E2	345919.26	−4.136	459.435	200	JPL
CH_3OH 5(4)− −6(3)−	346202.71	−4.662	115.162	129[m]	JPL
CH_3OH 5(4)+ − 6(3)+	346204.27	−4.662	115.162	129[m]	JPL
$^{13}CH_3OH$ 14(1,13)− 14(0,14) − +	347188.28	−3.360	254.251	96[b]	CDMS
CH_2DOH 3(2,1) − 2(1,2), e1	345718.71	−4.373	39.434	51	JPL
CH_2DOH 19(1,19) − 18(2,17), e1	345820.79	−4.531	418.032	B	JPL
CH_2DOH 22(4,19) − 22(3,19), e1	345850.48	−3.888	613.625	16[m]	JPL
CH_2DOH 3(1,2) − 3(0,3), e1	346256.50	−3.699	29.488	152	JPL
CH_2DOH 22(4,18) − 22(3,20), e1	346281.30	−3.874	613.621	16[m]	JPL
CH_2DOH 21(4,18) − 21(3,18), e1	346419.06	−3.886	566.562	13	JPL
CH_2DOH 21(4,17) − 21(3,19), e1	346783.70	−3.876	566.559	B	JPL
CH_2DOH 20(4,17) − 20(3,17), e1	346923.75	−3.886	521.634	85	JPL
CH_2DOH 20(4,16) − 20(3,18), e1	347222.99	−3.878	521.632	B	JPL
CH_2DOH 19(4,16) − 19(3,16), e1	347371.16	−3.887	478.841	18	JPL
CH_2DCN 20(1,20)−19(1,19)	345685.36	−2.444	179.628	12	JPL
CH_2DCN 20(0,20)−19(0,19)	347043.43	−2.438	174.955	27	JPL
CH_2DCN 20(4,17)−19(4,16)	347166.47	−2.455	261.246	13[m]	JPL
CH_2DCN 20(4,16)−19(4,15)	347166.48	−2.455	261.246	13[m]	JPL
CH_2DCN 20(2,19)−19(2,18)	347188.29	−2.441	196.562	B	JPL
CH_2DCN 20(3,18)−19(3,17)	347216.91	−2.447	223.527	B	JPL
CH_2DCN 20(3,17)−19(3,16)	347219.39	−2.447	223.527	B	JPL
CH_2DCN 20(2,18)−19(2,17)	347388.21	−2.441	196.615	24	JPL
CH_3CHO vt = 1, 18(2,17) − 17(2,16), E	346065.34	−2.838	371.350	90	JPL
CH_3CHO v = 0, 18(11,7) − 17(11,6), E	346697.59	−3.028	430.543	T	JPL
CH_3CHO v = 0, 18(10,8) − 17(10,7), E	346742.00	−2.986	383.352	16	JPL
CH_3CHO v = 0, 18(11,8) − 17(11,7), E	346754.52	−3.028	430.451	12[m]	JPL
CH_3CHO v = 0, 18(11,8) − 17(11,7), E	346755.92	−3.028	430.474	12[m]	JPL
CH_3CHO v = 0, 18(11,7) − 17(11,6), E	346755.92	−3.028	430.474	12[m]	JPL
CH_3CHO v = 0, 18(10,9) − 17(10,8), E	346763.91	−2.985	383.297	30	JPL
CH_3CHO v = 0, 18(9,9) − 17(9,8), E	346787.03	−2.950	340.618	B	JPL
CH_3CHO v = 0, 18(10,8) − 17(10,7), E	346805.46	−2.985	383.258	S	JPL
CH_3CHO v = 0, 18(10,9) − 17(10,8), E	346805.46	−2.985	383.258	S	JPL
CH_3CHO v = 0, 18(9,10) − 17(9,9), E	346807.99	−2.950	340.612	S	JPL
CH_3CHO v = 0, 18(8,10) − 17(8,9), E	346839.03	−2.920	302.406	23	JPL
CH_3CHO v = 0, 18(9,10) − 17(9,9), E	346849.06	−2.950	340.535	30[m]	JPL
CH_3CHO v = 0, 18(9, 9) − 17(9,8), E	346849.06	−2.950	340.535	30[m]	JPL
CH_3CHO v = 0, 18(8,11) − 17(8,10), E	346892.18	−2.920	302.343	S	JPL
CH_3CHO v = 0, 18(8,11) − 17(8,10), E	346893.81	−2.920	302.316	S	JPL
CH_3CHO v = 0, 18(8,10) − 17(8,9), E	346893.81	−2.920	302.316	S	JPL
CH_3CHO v = 0, 18(7,11) − 17(7,10), E	346934.22	−2.896	268.661	B	JPL
CH_3CHO v = 0, 18(7,12) − 17(7,11), E	346957.55	−2.896	268.606	B	JPL
CH_3CHO v = 0, 18(7,11) − 17(7,10), E	346957.55	−2.896	268.606	B	JPL
CH_3CHO v = 0, 18(7,12) − 17(7,11), E	346995.53	−2.896	268.572	24	JPL
CH_3CHO v = 0, 18(6,13)− 17(6,12), E	347071.54	−2.875	239.399	33[m]	JPL
CH_3CHO v = 0, 18(6,12) − 17(6,11), E	347071.68	−2.875	239.399	33[m]	JPL
CH_3CHO v = 0, 18(6,12) − 17(6,11), E	347090.40	−2.875	239.397	33[m]	JPL
CH_3CHO v = 0, 18(6,13) − 17(6,12), E	347132.68	−2.875	239.321	33	JPL
CH_3CHO vt = 1, 18(4,14) − 17(4,13), E	347182.41	−2.845	400.378	B	JPL
CH_3CHO vt = 1, 18(5,13) − 17(5,12), E	347216.79	−2.859	420.440	B	JPL
CH_3CHO vt = 1, 18(5,14) − 17(5,13), E	347251.82	−2.858	419.672	T	JPL
CH_3CHO v = 0, 18(5,14) − 17(5,13), E	347288.26	−2.858	214.697	53	JPL
CH_3CHO v = 0, 18(5,13) − 17(5,12), E	347294.87	−2.858	214.698	115	JPL
CH_3CHO v = 0, 18(5,13) − 17(5,12), E	347345.71	−2.858	214.640	B	JPL
CH_3CHO v = 0, 18(5,14) − 17(5,13), E	347349.27	−2.858	214.611	B	JPL

Table 1
(Continued)

Transition QNs	Frequency (MHz)	$\log(A_{ul})$ (s^{-1})	E_u (K)	W^a (K km s^{-1})	Line List
$HCOOCH_3$ v = 0 28(12,16)−27(12,15) E	345974.66	−3.287	335.433	11^m	JPL
$HCOOCH_3$ v = 0 28(12,17)−27(12,16) A	345985.38	−3.287	335.434	11^m	JPL
$HCOOCH_3$ v = 0 28(12,16)−27(12,15) A	345985.38	−3.287	335.434	11^m	JPL
$HCOOCH_3$ v = 0 28(12,17)−27(12,16) E	346001.61	−3.287	335.430	11^m	JPL
$HCOOCH_3$ v = 0 28(11,17)−27(11,16) E	346659.86	−3.269	320.394	B	JPL
$HCOOCH_3$ v = 0 28(11,18)−27(11,17) A	346674.98	−3.269	320.395	22^m	JPL
$HCOOCH_3$ v = 0 28(11,17)−27(11,16) A	346675.64	−3.269	320.396	22^m	JPL
$HCOOCH_3$ v = 0 28(11,18)−27(11,17) E	346687.46	−3.269	320.391	22^m	JPL
$HCOOCH_3$ v = 0 27(5,22)−26(5,21) E	347478.25	−3.211	247.252	B	JPL
$HCOOCH_3$ v = 0 27(5,22)−26(5,21) A	347493.96	−3.211	247.256	30	JPL
g−CH_3CH_2OH 20(3,18)−19(3,17) vt = 0−0	345648.57	−3.436	242.486	27	JPL
g−CH_3CH_2OH 20(10,10)−19(10, 9) vt = 1−1	346085.56	−3.549	358.843	T	JPL
g−CH_3CH_2OH 20(10,11)−19(10,10) vt = 1−1	346085.56	−3.549	358.843	T	JPL
g−CH_3CH_2OH 20(9,12)−19(9,11) vt = 1−1	346183.19	−3.522	335.566	T	JPL
g−CH_3CH_2OH 20(9,11)−19(9,10) vt = 1−1	346183.19	−3.522	335.566	T	JPL
g−CH_3CH_2OH 20(11,10)−19(11, 9) vt = 0−0	346383.64	−3.580	379.110	5^m	JPL
g−CH_3CH_2OH 20(11, 9)−19(11, 8) vt = 0−0	346383.64	−3.580	379.110	5^m	JPL
g−CH_3CH_2OH 20(10,11)−19(10,10) vt = 0−0	346424.58	−3.548	353.452	T	JPL
g−CH_3CH_2OH 20(10,10)−19(10, 9) vt = 0−0	346424.58	−3.548	353.452	T	JPL
g−CH_3CH_2OH 20(9,12)−19(9,11) vt = 0−0	346505.34	−3.521	330.252	T	JPL
g−CH_3CH_2OH 20(9,11)−19(9,10) vt = 0−0	346505.34	−3.521	330.252	T	JPL
g−CH_3CH_2OH 20(7,14)−19(7,13) vt = 1−1	346565.08	−3.479	296.366	22^m	JPL
g−CH_3CH_2OH 20(7,13)−19(7,12) vt = 1−1	346565.39	−3.479	296.366	22^m	JPL
g−CH_3CH_2OH 20(8,13)−19(8,12) vt = 0−0	346620.32	−3.498	309.511	T	JPL
g−CH_3CH_2OH 20(8,12)−19(8,11) vt = 0−0	346620.33	−3.498	309.511	T	JPL
g−CH_3CH_2OH 20(7,14)−19(7,13) vt = 0−0	346816.58	−3.478	291.241	12^m	JPL
g−CH_3CH_2OH 20(7,13)−19(7,12) vt = 0−0	346816.92	−3.478	291.241	12^m	JPL
t−CH_3CH_2OH 21(0,21)−20(1,20)	346962.59	−3.616	185.843	B	JPL
g−CH_3CH_2OH 20(6,15)−19(6,14) vt = 0−0	347147.20	−3.461	275.456	13	JPL
g−CH_3CH_2OH 20(6,14)−19(6,13) vt = 0−0	347157.99	−3.461	275.457	9	JPL
t−CH_3CH_2OH 14(3,12)−13(2,11)	347350.92	−3.757	99.660	B	JPL
t−CH_3CH_2OH 21(1,21)−20(0,20)	347445.52	−3.573	185.853	41	JPL
g−CH_3CH_2OH 20(5,16)−19(5,15) vt = 1−1	347473.56	−3.447	267.087	B	JPL

Notes.
[a] Integrated line intensities (see the text for the definition) measured from the lower disk atmosphere for the reasonably isolated lines detected with more than 3σ. They are the mean values averaging over a rectangular region (with a size of $0\farcs2 \times 0\farcs05$ covering most of the emission) centered at the lower atmosphere. In this column, the line intensities commented with "*m*" are the mean values obtained by averaging over two or more lines with similar E_u and log A_{ul} for better measurements. T: the lines are tentatively detected with about 2σ detection and a part of the linear PF structure. S: the lines are blended with the line(s) of the same molecule at different transitions. B: the lines are blended with the line(s) of other molecules. The line intensities here are assumed to have an uncertainty of 40%.
[b] $^{13}CH_3OH$ intensity after removing the small contribution from CH_2DCN (see the text).

to those in IRAS 16293-2422B (Jørgensen et al. 2018), B335 (Imai et al. 2016), and NGC 1333 IRAS4A2 (López-Sepulcre et al. 2017). In this comparison, CH_3SH is excluded because of no reliable measurement of this molecule in other hot corinos to compare with. Interestingly, the relative abundances of most molecules here in HH 212 are similar to those in other hot corinos to within a factor of few, suggesting that the formation of these molecules in the disk atmosphere could be similar to that in other hot corinos. Notice that the abundance of CH_3SH here is also consistent with that predicted in the hot corino, which can be as high as 5×10^{-8} (Majumdar et al. 2016). Moreover, the abundances here are also similar to those seen in the Class I corino SVS13-A (Bianchi et al. 2019) and to those seen in Comet Lovejoy, which shows similar abundances to IRAS 16293-2422B (Biver et al. 2015).

As discussed in Lee et al. (2017c), the high degree of deuteration in methanol (with $[CH_2DOH]/[CH_3OH]$ ∼0.12) and the detection of doubly deuterated formaldehyde suggest that the methanol and formaldehyde in the disk atmosphere are originally formed on icy grains and later desorbed (evaporated) into gas phase due to the heating possibly by low-velocity accretion shock near the centrifugal barrier or the radiation of the protostar. This heating can also be produced by an interaction with a wind/outflow from an inner region (Lee et al. 2018). The temperature of the disk atmosphere where the organic molecules are detected is similar to the freeze-out temperature of water, which is ∼150 K (Öberg et al. 2011). Thus, the detection of deuterated water in the disk atmosphere (Codella et al. 2018) supports that the two organic molecules are evaporated in the disk atmosphere where it is warm enough to release the water. However, how the other organic molecules are formed is still an open question and not necessarily on the grain surfaces.

In case the organic molecules are formed on the icy grains, they can be formed on the icy grains in the disk, as suggested in the TW Hya protoplanetary disk for the methanol (Walsh et al.

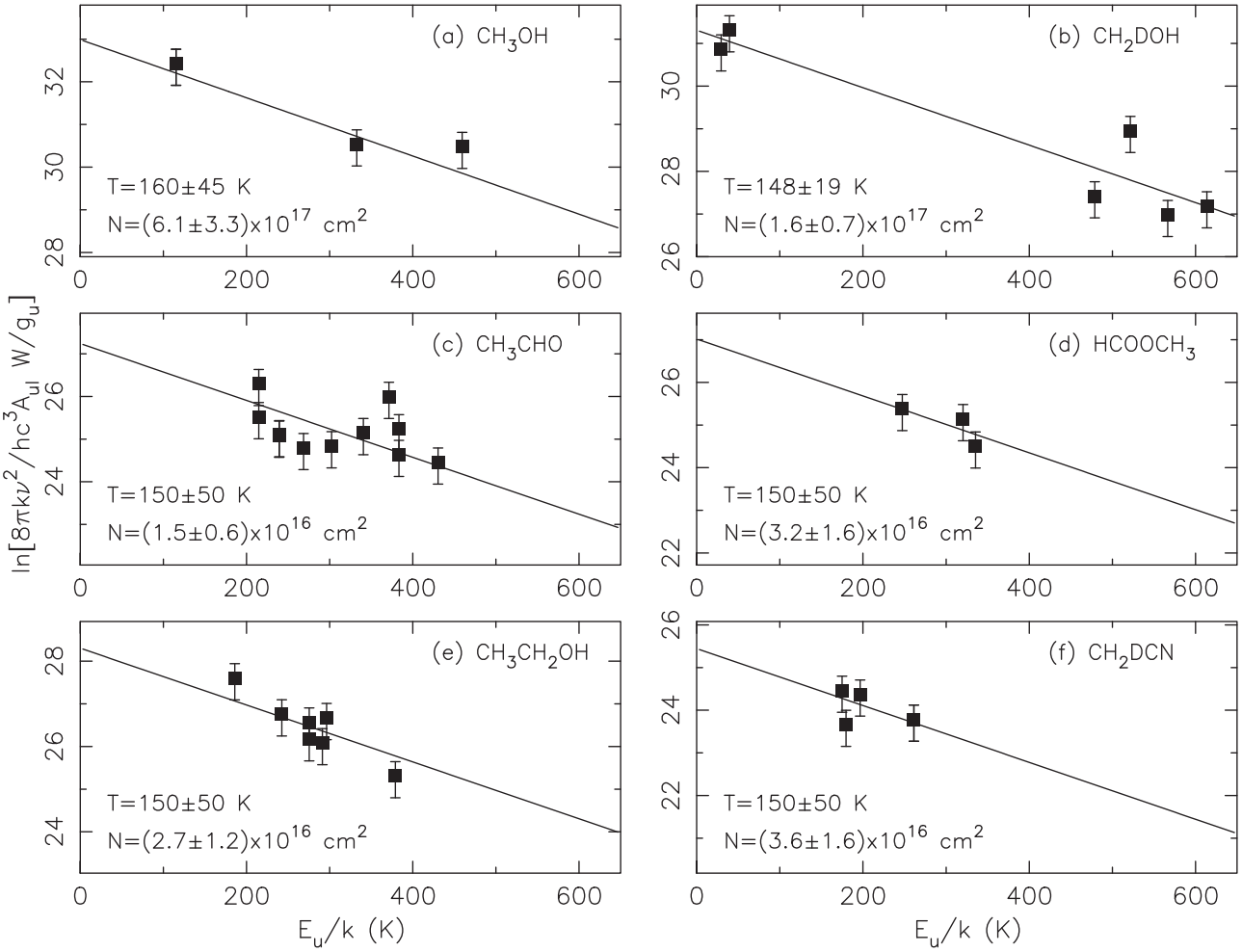

Figure 3. Rotation diagrams for molecular lines of the six organic molecules including CH_3OH, CH_2DOH, CH_3CHO, $HCOOCH_3$, CH_3CH_2OH, and CH_2DCN. The diagrams are derived from the line intensities in the lower disk atmosphere listed in Table 1. The error bars show the uncertainty in our measurements, which are assumed to be 40% of the data values. The solid line is a linear fit to the data. In panels (c)–(f), the temperature is fixed at 150 ± 50 K for the fitting in order to derive the column densities from the weak lines.

2016), either in situ on the surface or first in the midplane and then brought to the surface by turbulence (Furuya & Aikawa 2014). Like the hot corinos, it is also possible that the molecules already formed on the icy grains in the prestellar core, and then were brought in to the disk surface. CO is frozen onto to the grains at the temperature of ∼20 K (Öberg et al. 2011). One possible scenario (although to be proven) is that, in the regions such as prestellar cores and probably the disk midplane where the temperature is below 20 K, CO-rich ices on dust grains can undergo addition reactions with H (and D), O, C, and N atoms accreted from the gas, producing a rich organic chemistry on the grains, as proposed in Charnley & Rodgers (2008).

Having said that, some of the organic molecules could also be quickly formed in the gas phase using simpler species released from grains. This could be the case for formamide, which was found to be mainly formed in the gas phase in a young shocked region such as L1157-B1 (Codella et al. 2017). In addition, acetaldehyde can also be formed in gas phase, as suggested in Charnley (2004).

These organic molecules are of great importance for forming even more COMs such as amino acids and amino sugars, which are the building blocks of life. Our observations clearly show that they have formed in a disk or been brought in to a disk in the earliest phase of star formation and may play a crucial role in producing the rich organic chemistry needed for life. It is also tempting to estimate the alcohol degree in the disk atmosphere. According to Codella et al. (2018), the column density of deuterated water is $\lesssim 3 \times 10^{17}$ cm^{-2}. Assuming [H/D] ∼ [CH_3OH/CH_2DOH] ∼ 8.1, then the column density of the water is $\lesssim 2.4 \times 10^{18}$ cm^{-2}. With the derived column density of ethanol in Table 2, and the molecular mass of ethanol of 46 and water of 18, the alcohol degree by mass is estimated to be $\gtrsim$2.8%, and thus could be similar to that of a regular beer.

4.3. Possible Disk Wind?

Methanol and acetaldehyde have been argued to trace a disk wind in HH 212 (Leurini et al. 2016; Codella et al. 2018). Now in observations at higher resolution, they seem to trace mainly a ring of disk atmosphere near the centrifugal barrier, which could in principle be heated by a weak (accretion) shock produced by the rapid decrease of the infall velocity near the centrifugal barrier. However, as their maps also show small extensions extending out from the disk (see Figure 1), they may also trace a wind coming out from the disk surface. Nonetheless, as these extensions appear to be surrounding the

Table 2
Column Densities and Abundances in the Lower Disk Atmosphere

Species	Excitation Temperature (K)	Column Density (cm^{-2})	Abundance[a]
CH_3OH...[b]	160 ± 45	$(6.1 \pm 3.3) \times 10^{17}$	$(1.6 \pm 0.9) \times 10^{-7}$
CH_3OH...[c]	150 ± 50[d]	$(1.3 \pm 0.7) \times 10^{18}$	$(3.3 \pm 1.8) \times 10^{-7}$
CH_2DOH	148 ± 19	$(1.6 \pm 0.7) \times 10^{17}$	$(4.2 \pm 1.8) \times 10^{-8}$
$^{13}CH_3OH$[e]	150 ± 50[d]	$(2.5 \pm 1.4) \times 10^{16}$	$(6.6 \pm 3.7) \times 10^{-9}$
H_2CCO	150 ± 50[d]	$(3.8 \pm 2.0) \times 10^{15}$	$(1.0 \pm 0.5) \times 10^{-9}$
t-HCOOH	150 ± 50[d]	$(2.0 \pm 1.1) \times 10^{16}$	$(5.3 \pm 2.9) \times 10^{-9}$
CH_2DCN	150 ± 50[d]	$(3.6 \pm 1.6) \times 10^{14}$	$(9.5 \pm 4.2) \times 10^{-11}$
CH_3CHO	150 ± 50[d]	$(1.5 \pm 0.6) \times 10^{16}$	$(3.9 \pm 1.6) \times 10^{-9}$
$HCOOCH_3$	150 ± 50[d]	$(3.2 \pm 1.6) \times 10^{16}$	$(8.4 \pm 4.2) \times 10^{-9}$
CH_3CH_2OH	150 ± 50[d]	$(2.7 \pm 1.2) \times 10^{16}$	$(7.1 \pm 3.2) \times 10^{-9}$
CH_3SH[f]	150 ± 50[d]	$(9.3 \pm 5.5) \times 10^{16}$	$(2.4 \pm 1.4) \times 10^{-8}$
NH_2CHO[f]	150 ± 50[d]	$(1.6 \pm 0.9) \times 10^{15}$	$(4.2 \pm 2.4) \times 10^{-10}$
D_2CO[f]	150 ± 50[d]	$(3.0 \pm 1.6) \times 10^{15}$	$(7.9 \pm 4.2) \times 10^{-10}$

Notes.
[a] Derived by dividing the column densities of the molecules by the H_2 column density in the disk atmosphere, which is $\sim 3.8 \times 10^{24}$ cm^{-2} (see the text).
[b] Derived from the rotation diagram in Figure 3(a). The value derived this way is considered as the lower limit of the CH_3OH column density (see the text).
[c] Obtained by multiplying the $^{13}CH_3OH$ column density by 50, which is the $^{12}C/^{13}C$ ratio obtained in the Orion complex (Kahane et al. 2018). The value derived this way is adopted for the CH_3OH column density (see the text).
[d] Assuming an excitation temperature (rotational temperature) of 150 ± 50 K, which is the mean value derived from the CH_3OH and CH_2DOH lines.
[e] Estimated after subtracting the small contribution from CH_2DCN (see the text).
[f] Adopted from Lee et al. (2017c), updated for an excitation temperature of 150 ± 50 K.

SO outflow shell detected further in Lee et al. (2018), they could also be the disk atmosphere pushed away by the SO outflow shell. Detailed kinematic study of these extensions with the SO outflow shell is needed to check these scenarios.

5. Conclusions

The nearly edge-on orientation of the disk in HH 212 provides the best view of the disk atmosphere. Here we have detected 9 organic molecules in the disk atmosphere. These molecules are characteristic of a hot corino and are found here to be in the disk atmosphere, confirming that the corino here is a warm disk atmosphere. Adding 3 other organic molecules from our previous study, we have detected 12 organic molecules, with 9 of them being COMs, in the disk atmosphere within ~40 au of the central protostar. These molecules seem to arise mainly from a ring of disk atmosphere near the centrifugal barrier. Some of them may also trace a wind coming out from the disk surface.

The relative abundances of the organic molecules in the HH 212 disk atmosphere are similar to those in hot corinos around other low-mass protostars and even to those in Comet Lovely. It would be interesting to determine whether the hot corinos around other low-mass protostars are also located in their disk atmospheres or not, perhaps through higher-resolution ALMA observations. In addition, the formation mechanism of the organic molecules can also be similar to that in those corinos. The organic molecules can originally be formed on icy grains, either in the disk or in the prestellar core and then brought in to the disk, and then desorbed (evaporated) into the gas phase. They can also be quickly formed in the gas phase using simpler species ejected from the dust mantles.

We thank the anonymous referee for constructive comments. This paper makes use of the following ALMA data: ADS/JAO.ALMA#2017.1.00044.S. ALMA is a partnership of ESO (representing its member states), NSF (USA) and NINS (Japan), together with NRC (Canada), NSC and ASIAA (Taiwan), and KASI (Republic of Korea), in cooperation with the Republic of Chile. The Joint ALMA Observatory is operated by ESO, AUI/NRAO and NAOJ. C.-F.L. acknowledges grants from the Ministry of Science and Technology of Taiwan (MoST 104-2119-M-001-015-MY3 and 107-2119-M-001-040-MY3) and the Academia Sinica (Career Development

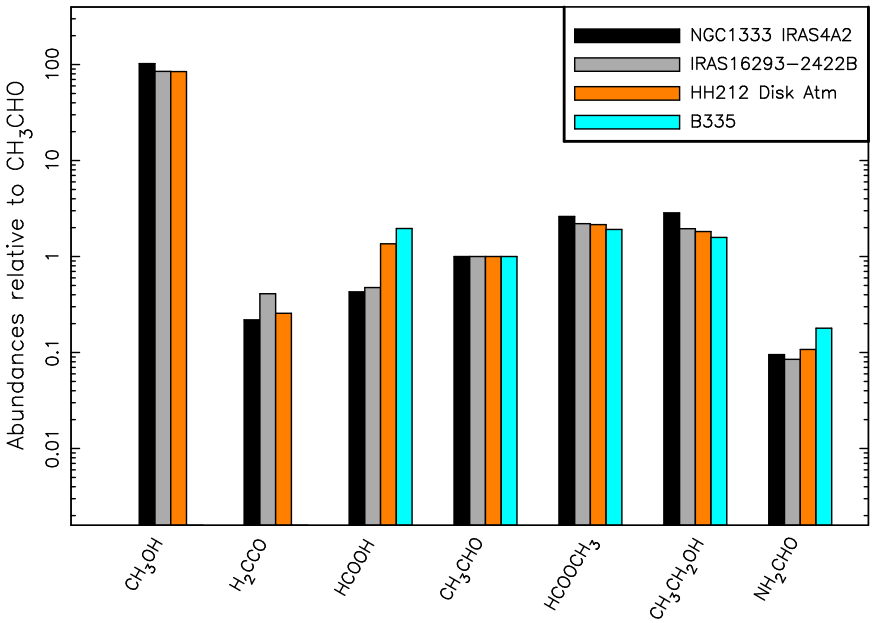

Figure 4. Comparison of the abundances of organic molecules in the HH 212 disk atmosphere with those in the hot corinos around other low-mass protostars. As shown in Table 2, our measurements have an uncertainty of about 50%.

Award and Investigator Award). C.C. acknowledges the project PRIN-INAF 2016 The Cradle of Life—GENESIS-SKA (General Conditions in Early Planetary Systems for the rise of life with SKA). Z.-Y.L. is supported in part by NSF grants AST-1815784 and ASTR-1716259 and NASA grants 80NSSC18K1095 and NNX14AB38G.

ORCID iDs

Chin-Fei Lee https://orcid.org/0000-0002-3024-5864
Claudio Codella https://orcid.org/0000-0003-1514-3074
Sheng-Yuan Liu https://orcid.org/0000-0003-4603-7119

References

Bianchi, E., Codella, C., Ceccarelli, C., et al. 2017, MNRAS, 467, 3011
Bianchi, E., Codella, C., Ceccarelli, C., et al. 2019, MNRAS, 483, 1850
Biver, N., Bockelée-Morvan, D., Moreno, R., et al. 2015, SciA, 1, 1500863
Bizzocchi, L., Caselli, P., Spezzano, S., & Leonardo, E. 2014, A&A, 569, A27
Ceccarelli, C., Caselli, P., Herbst, E., Tielens, A. G. G. M., & Caux, E. 2007, in Protostars and Planets V, ed. B. Reipurth, D. Jewitt, & K. Keil (Tucson, AZ: Univ. Arizona Press), 47
Charnley, S. B. 2004, AdSpR, 33, 23
Charnley, S. B., & Rodgers, S. D. 2008, SSRv, 138, 59
Claussen, M. J., Marvel, K. B., Wootten, A., & Wilking, B. A. 1998, ApJL, 507, L79
Codella, C., Bianchi, E., Tabone, B., et al. 2018, A&A, 617, A10
Codella, C., Ceccarelli, C., Cabrit, S., et al. 2016, A&A, 586, L3
Codella, C., Ceccarelli, C., Caselli, P., et al. 2017, A&A, 605, L3
Furuya, K., & Aikawa, Y. 2014, ApJ, 790, 97
Herbst, E., & van Dishoeck, E. F. 2009, ARA&A, 47, 427
Imai, M., Sakai, N., Oya, Y., et al. 2016, ApJL, 830, L37
Jørgensen, J. K., Müller, H. S. P, Calcutt, H., et al. 2018, A&A, 620, A170
Jørgensen, J. K., van der Wiel, M. H. D., Coutens, A., et al. 2016, A&A, 595, A117
Kahane, C., Jaber Al-Edhari, A., Ceccarelli, C., et al. 2018, ApJ, 852, 130
Kounkel, M., Hartmann, L., Loinard, L., et al. 2017, ApJ, 834, 142
Lee, C.-F., Hirano, N., Zhang, Q., et al. 2014, ApJ, 786, 114
Lee, C.-F., Hirano, N., Zhang, Q., et al. 2015, ApJ, 805, 186
Lee, C.-F., Ho, P. T. P., Li, Z.-Y., et al. 2017a, NatAs, 1, 0152
Lee, C.-F., Li, Z.-Y., Codella, C., et al. 2018, ApJ, 856, 14
Lee, C.-F., Li, Z.-Y., Ho, P. T. P., et al. 2017b, SciA, 3, e1602935
Lee, C.-F., Li, Z.-Y., Ho, P. T. P., et al. 2017c, ApJ, 843, 27
Leurini, S., Codella, C., Cabrit, S., et al. 2016, A&A, 595, L4
López-Sepulcre, A., Sakai, N., Neri, R., et al. 2017, A&A, 606, A121
Majumdar, L., Gratier, P., Vidal, T., et al. 2016, MNRAS, 458, 1859
Milam, S. N., Savage, C., Brewster, M. A., Ziurys, L. M., & Wyckoff, S. 2005, ApJ, 634, 1126
Öberg, K. I., Murray-Clay, R., & Bergin, E. A. 2011, ApJL, 743, L16
Walsh, C., Loomis, R. A., Öberg, K. I., et al. 2016, ApJL, 823, L10
Zinnecker, H., Bastien, P., Arcoragi, J.-P., & Yorke, H. W. 1992, A&A, 265, 726
Zinnecker, H., McCaughrean, M. J., & Rayner, J. T. 1998, Natur, 394, 862